Dipole strength in ^{78}Se below the neutron separation energy from a combined analysis of ^{77}Se(n, γ) and ^{78}Se(γ, γ') experiments

G. Schramm,[1] R. Massarczyk,[1] A. R. Junghans,[1] T. Belgya,[2] R. Beyer,[1] E. Birgersson,[1,*] E. Grosse,[1,3] M. Kempe,[1,3] Z. Kis,[2] K. Kosev,[1,†] M. Krtička,[4] A. Matic,[1,‡] K. D. Schilling,[1] R. Schwengner,[1] L. Szentmiklósi,[2] A. Wagner,[1] and J. L. Weil[2]

[1]*Helmholtz-Zentrum Dresden-Rossendorf, Institute of Radiation Physics, D-01328 Dresden, Germany*

[2]*Hungarian Academy of Sciences, Institute of Isotopes, H-1525 Budapest, Hungary*

[3]*Technische Universität Dresden, Institute of Nuclear and Particle Physics, D-01062 Dresden, Germany*

[4]*Charles University, Faculty of Mathematics and Physics, CZ-180 00 Prague 8, Czech Republic*

(Received 24 October 2011; published 17 January 2012)

The dipole strength function and the nuclear level density of the compound nucleus ^{78}Se were studied in a combined analysis of a cold neutron capture experiment on ^{77}Se performed at the research reactor in Budapest and a photon-scattering experiment on ^{78}Se performed at the electron linear accelerator ELBE with bremsstrahlung produced at a kinetic electron energy of 11.5 MeV. In the combined analysis we developed the extreme statistical code γDEX for the simulation of radiative cascade deexcitations occurring in neutron capture and photon scattering. Comparisons of experimental and simulated neutron capture spectra allow us to estimate a temperature of $T = 900$ keV for the level density according to the constant-temperature model for ^{78}Se. Using γDEX, we were also able to estimate ground-state branching ratios and intensities of inelastic transitions for states in ^{78}Se excited via photon scattering. In this way, we derived the photoabsorption cross section from 4 MeV up to the neutron separation energy from the measured photon-scattering data. The results obtained match the photoabsorption cross section derived from (γ, n) measurements and show an enhancement of dipole strength around 9 MeV.

DOI: 10.1103/PhysRevC.85.014311 PACS number(s): 21.10.Ma, 24.60.Dr, 25.20.Dc, 25.40.Lw

I. INTRODUCTION

Radiative capture of neutrons is of special importance for the transmutation of high-level radioactive waste. Knowledge of the respective cross sections is essential for the technical design of future transmutation systems [1] especially when capture channels compete with fission. In most cases thermal and cold neutron capture leads to compound nucleus formation followed by a γ-ray cascade deexcitation toward the ground state. In photon scattering, nuclei are excited via the absorption of real photons. If the excitation energy is below the neutron threshold (S_n), these nuclei also deexcite back to the ground state via a γ-ray cascade. In both experimental cases information about the photon strength function (PSF) and the nuclear level density (LD), which govern the transition probabilities of the excited states, can be deduced.

Recently [2], a global parametrization of the electric dipole strength function in heavy nuclei has been proposed. It shows that for $A > 80$ the electric dipole strength is well characterized as the low-energy tail of the isovector giant dipole resonance (GDR). Its resonance integral, which determines the energy-integrated photoabsorption cross section, is assumed to be in accordance with the Thomas-Reiche-Kuhn sum rule [3] and its spreading width is well parametrized as a function of its resonance energy. The centroid energy of the GDR is predictable using parameters determined from nuclear ground-state masses using the finite-range droplet model (FRDM). The splitting of the GDR into three Lorentzian components induced by the deviation of the nuclear shape from spherical symmetry has to be taken from nuclear spectroscopic data. The splitting has an impact on the energy dependence of the capture cross section because it considerably influences the low-energy tail of the GDR. Moreover, the triple Lorentzian model (TLO) concept [2] can be used to describe the electric dipole strength function derived from photoneutron, photon-scattering, and averaged resonance neutron capture studies.

In the past, neutron capture and photon-scattering data have been interpreted in several different ways [4]. Disagreeing predictions for PSFs have been in use by the two communities of neutron and photon beam experimenters as visible in the IAEA reference input parameter library RIPL-2 [5], where six different analytical formulas based on capture data are listed for the calculation of $E1$ PSFs. Further investigations are urgently needed because the microscopically calculated $E1$ PSFs given there are at variance to many neutron capture data as well as photon-scattering data [2].

In the recently started RIPL-3-initiative [6] some of these deficiencies have been worked on, but the correlation between GDR width and nuclear triaxiality [2] is not properly accounted for. One reason for the contradiction between the parametrizations resulting from photon-scattering data compared to that from neutron capture data may be the fact that often different spins are populated in the two reactions, making a direct comparison of these data difficult. This difference can be minimized by using spin $1/2^-$ nuclei with ^{A}Z for neutron capture to be compared to photon-scattering data from ^{A+1}Z. In this case, 1^- states are mainly populated in both

*Present address: Areva NP GmbH, D-91052 Erlangen, Germany.

†Present address: Bosch Solar Energy AG, D-99310 Arnstadt, Germany.

‡Present address: IBA Particle Therapy, D-45157 Essen, Germany.

experiments. Unfortunately, only very few such pairs of stable nuclei are available as targets for the two types of experiments.

In the present work the above-mentioned reactions are investigated for the pair ^{77}Se-^{78}Se. It is the aim of this paper to investigate to what extent neutron capture and photon scattering can be described using the same PSF and LD. In the following, Sec. II is a brief description of the two experiments and Sec. III focuses on the statistical description of radiative deexcitation spectra. The simulation code γDEX is discussed in detail in Sec. IV, and finally Sec. V describes the determination of the average photoabsorption cross section deduced from the photon-scattering data.

II. EXPERIMENTAL SETUPS

A. The neutron capture experiment

A neutron capture experiment on ^{77}Se was performed at the 10-MW$_{\text{th}}$ research reactor of the Hungarian Academy of Sciences in Budapest. Neutrons from a cold neutron source with a mean kinetic energy of approximately 6 meV, guided by a bent beam tube consisting of neutron super mirrors to the prompt gamma activation analysis (PGAA) measurement station [7], were used for radiative capture. The thermal equivalent neutron flux at the target position was approximately 10^8 cm^{-2} s^{-1}.

A bismuth germanate (BGO) escape-suppression-shielded Ortec GMX 100 S high-purity germanium (HPGe) detector with a relative efficiency of 100% mounted at 90° with respect to the beam axis was used for γ-ray detection. The detector was covered with lead and ^{6}Li-filled plastic sheets to reduce the background count rate. The beam background from neutron capture on structural materials was measured with a blank target. The count rate in the blank target experiment was 150 counts/s, which compares to 2000 counts/s when the target enriched to 99.66% in ^{77}Se was put into the beam. The measured and detector-response-corrected ^{77}Se(n,γ) spectra are shown in Fig. 1. We sequentially subtracted response spectra of monoenergetic γ rays simulated in GEANT4 [8] in steps of 10 keV starting at the high-energy end of the measured spectrum to deconvolve the measured spectrum for detector

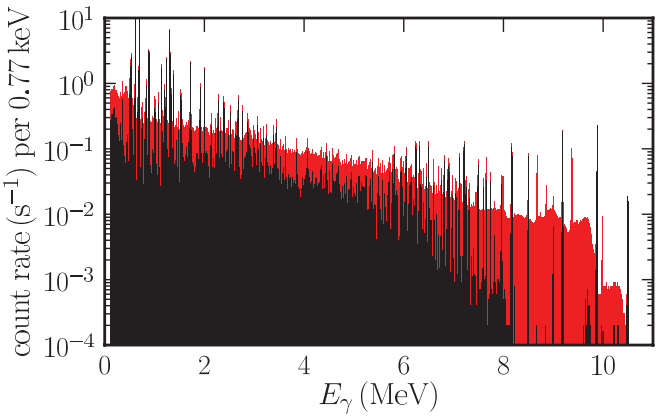

FIG. 1. (Color online) Measured (red) and detector-response-corrected spectrum (black) in the ^{77}Se(n,γ) reaction.

response. Moreover, a combination of these simulations and source measurements was used to obtain the efficiency of the HPGe detector.

Additionally, we performed a capture experiment on deuterated urea to test the detector response deconvolution. The same deconvolution algorithm was applied to the urea spectrum. Subsequently, we normalized the corrected spectrum to the partial cross section of the 10.83-MeV transition following neutron capture on ^{14}N and compared the corrected normalized summed intensity of the spectrum to the summed partial cross section of all transitions in N, O, C, ^{1}H, and ^{2}H and transitions from structural background contributions of Fe, Cu, Cl, Al, Pb, and ^{6}Li above 2.4 MeV from Ref. [9]. We found a difference of 4% between the response-and-efficiency-corrected spectrum and the tabulated values. Assuming conservation of energy, we additionally calculated the total capture cross section σ_γ,

$$\sigma_\gamma S_n = \sum_i \sigma_i E_i, \tag{1}$$

from the detector-response-and-efficiency-corrected ^{77}Se spectrum normalized to σ_i of the 9.88-MeV transition in ^{78}Se [9]. In Eq. (1) σ_i is the partial cross section for a γ transition with energy E_i following neutron capture. We determined a value of

$$\sigma_\gamma = 36(4/2)\ \text{b}, \tag{2}$$

where the first uncertainty is due to the uncertainty of the 9.88-MeV transition and the second one is due to uncertainty in the response deconvolution. The obtained value is in agreement with $\sigma_\gamma = 42(4)$ b given in Ref. [10], but it should be noted that approximately half of the cross section in Eq. (2) is coming from the deconvoluted continuum, and not from resolved photopeaks. The agreement between the calculated and the literature value of σ_γ proves the correctness of our algorithm for detector response and efficiency correction.

Regarding the shape of the corrected experimental ^{77}Se(n,γ) spectrum, distinct peaks from transitions from the capture state after cold neutron capture to several of the lowest excited states in the compound nucleus ^{78}Se are resolved in the high-energy region of the spectrum ($7.5 < E_\gamma \leqslant S_n = 10.5$ MeV). In the intermediate region ($2 < E_\gamma \leqslant 7.5$ MeV), a quasicontinuum of unresolved and resolved transitions can be seen. This quasicontinuum consists of weak transitions which are not resolvable due to the finite energy resolution of the detector. The low-energy region of the spectrum ($0 < E_\gamma \leqslant 2$ MeV) is dominated by transitions between the lowest well-separated excited states in the compound nucleus appearing in the last steps of a cascade deexcitation. The most prominent peak appears at 613 keV, corresponding to the ground-state transition from the first 2^+ state in ^{78}Se. The further analysis below is concentrated on a statistical simulation of the capture γ spectrum. In particular, the influence of PSF and LD on the shape of the quasicontinuum region will be investigated.

B. The photon-scattering experiment

Complementary to the radiative-capture experiment on ^{77}Se, a photon-scattering experiment on ^{78}Se was performed

using the bremsstrahlung facility [11] at the superconducting electron accelerator ELBE at Helmholtz-Zentrum Dresden-Rossendorf (HZDR). Bremsstrahlung was produced by an electron beam of 11.5-MeV kinetic energy and an average current of 520 μA hitting a 4-μm-thick niobium radiator. A beam of bremsstrahlung shaped by an Al collimator of 2.6 m in length with a conical hole of 8 mm at the entrance and 24 mm at the exit was used for photoexcitation of the target. To increase the intensity ratio of the high-energy to the low-energy part of the bremsstrahlung spectrum at the target position a cylindrical Al absorber of 100 mm in length was placed in front of the collimator. At the target position the collimated beam had a size of approximately 38 mm in diameter and a spectral photon flux of approximately 10^7 MeV^{-1} cm^{-2} s^{-1} at 8.9 MeV.

The target consisted of 2002 mg of ^{78}Se enriched to 99.39% sandwiched between disks of 212.5 and 105.6 mg of ^{11}B enriched to 99.5% used for the determination of the photon fluence. The three target disks had a diameter of 20 mm to assure a constant photon flux over the target area.

Four HPGe detectors of 100% relative efficiency were used to detect scattered photons. The HPGe detectors were equipped with escape-suppression shields consisting of BGO scintillation detectors. Lead collimators of 10 cm thickness were placed in front of the detectors to suppress background radiation scattered from surrounding materials. The BGO detectors were cylindrically encapsulated by 2-cm-thick lead layers. Two detectors were placed vertically at 90° relative to the beam direction at a distance of 28 cm from the target. The other two detectors were placed horizontally at 127° relative to the beam axis at a distance of 32 cm from the target. Additional absorbers made of 13 mm of Pb plus 3 mm of Cu and 8 mm of Pb plus 3 mm of Cu were placed in front of the detectors at 90° and 127°, respectively, to reduce the amount of scattered low-energy photons. A spectrum measured with both detectors at 127° is shown in Fig. 2.

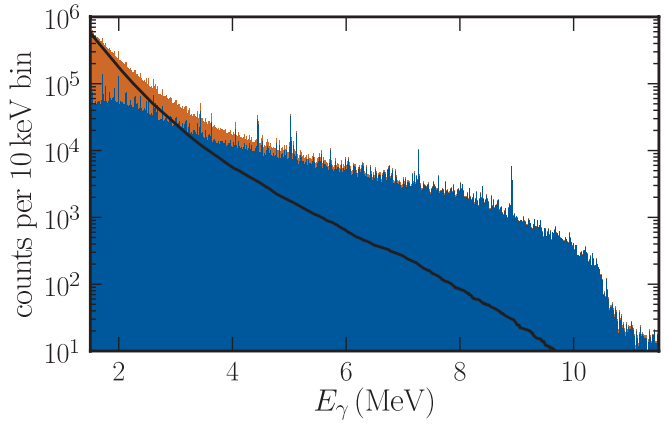

FIG. 2. (Color online) Spectrum of photons scattered from ^{78}Se, measured at 127° relative to the incident beam, corrected for room background and detector response (orange bars), compared to the simulated spectrum of the atomic background (black line), multiplied with efficiency and measuring time. The blue spectrum results from a subtraction of the atomic background from the experimental spectrum. The prominent peaks at 4.44, 5.02, 7.29, and 8.91 MeV are transitions in ^{11}B.

III. STATISTICAL DESCRIPTION OF RADIATIVE EXCITATION SPECTRA

A. Neutron capture γ spectra

The γ-ray spectra from (cold) neutron capture reveal interesting information about the structure of nuclei. As will be shown, they are sensitive to the nuclear level density as well as to radiative properties such as PSFs of the compound nucleus. The process of neutron capture can be visualized as a two-step process. In the first step, a neutron is captured by a target nucleus (TN) with $^A Z$ leading to an excited compound nucleus (CN) with $^{A+1} Z$. In cold neutron capture, the excitation energy of the CN is approximately equal to the neutron separation energy S_n.

Possible spins J_{CN} of the excited CN after s-wave neutron capture are $|J_{TN} - 1/2|$ and $J_{TN} + 1/2$, where J_{TN} is the ground-state spin of the TN. The parity of the excited state is given by $\Pi_n \Pi_{TN}$, where $\Pi_n = +1$ is the parity of the s-wave neutron and Π_{TN} is the ground-state parity of the TN. In cold neutron capture, where the mean kinetic energy and the energy spread of the incident neutron spectrum is very small compared to the mean resonance spacing of the CN at S_n, it is assured that mainly the nearest s-wave resonance to S_n is excited. For the case of ^{77}Se(n, γ) this is a 1^- resonance at 10.498 MeV according to Ref. [10].

In the second step after the capture process, the excited CN deexcites back to the ground state via the emission of γ radiation. This deexcitation process can either happen in a direct ground-state transition, leading to the emission of a single γ ray with energy $E_\gamma \approx S_n$, or in a so-called cascade deexcitation in which different intermediate states of the excited nucleus are populated, leading to the emission of several γ rays with summed transition energy S_n. If one knew the energies and transition probabilities which are related to the transition widths between all excited states in the CN up to S_n, a prediction of the neutron capture γ-ray spectrum would theoretically be possible. However, in reality this is not feasible for several reasons:

(i) The energies and transition widths in medium and heavy nuclei are known only in the low-energy region ($E_{ex} \lesssim 3$ MeV) from nuclear spectroscopy.
(ii) The number of excited states in nuclei increases exponentially. For example, in ^{78}Se there are in total approximately 10^5 states up to S_n.
(iii) The transition widths strongly fluctuate around their mean, implying that many weak transitions are below the detection threshold.

Therefore, it is only possible to use an extreme statistical ansatz that the number of counts in a energy bin ΔE in an experimentally measured neutron capture γ spectrum results from various transitions between various initial and final states. Using this assumption makes it valid to calculate and use average values of the transition widths for the description of the deexcitation spectrum.

In general, the number of emitted primary γ rays, $Y_{\rm bin}$, from an initially excited state i ending in a finite energy bin $[E_f - \frac{\Delta}{2}, E_f + \frac{\Delta}{2}]$ is proportional to

$$Y_{\rm bin} \propto \sum_{f', E_{f'} \in {\rm bin}} \frac{\Gamma_{if'}}{\Gamma_{i,{\rm tot}}} = \sum_{f', E_{f'} \in {\rm bin}} \frac{y_{if'} \langle \Gamma_{if'} \rangle}{\Gamma_{i,{\rm tot}}}, \qquad (3)$$

where $\Gamma_{if'}$ is the partial transition width from i to a final state f' and $\Gamma_{i,{\rm tot}}$ is the total radiative width of i. In the right part of Eq. (3), $\Gamma_{if'}$ is expressed by its mean value $\langle \Gamma_{if'} \rangle$ times a random number $y_{if'}$, which describes the fluctuation of the transition widths. If, on the one hand, the energy bin is big enough to assure that there are many possible final states in the bin and on the other hand it is small enough so that the mean transition width does not vary too much over the bin, one obtains

$$Y_{\rm bin} \propto \frac{\langle \Gamma_{if} \rangle}{\Gamma_{i,{\rm tot}}} \sum_{f', E_{f'} \in {\rm bin}} y_{if'} \approx N_{\rm bin} \frac{\langle \Gamma_{if} \rangle}{\Gamma_{i,{\rm tot}}}. \qquad (4)$$

In the right part of Eq. (4), the sum over all fluctuation factors was replaced by the number of final states in the bin, $N_{\rm bin}$, which is justified if there is a sufficiently high number of possible final states in the bin so that the fluctuations cancel out. This is the case for transitions to the quasicontinuum, but not for ones to low-lying excited states. Finally, by using the definition of the PSF given in Ref. [12] for replacing the average transition width one obtains for the spectral distribution of primary γ rays

$$Y_{{\rm bin},XL}(E_\gamma) \propto \varrho_{XL}(E_i - E_\gamma) \frac{f_{XL}(E_\gamma)\, E_\gamma^{2L+1}}{\Gamma_{i,{\rm tot}}\, \varrho(E_i)}, \qquad (5)$$

where XL defines the type of multipole radiation with X standing for electric (E) or magnetic (M) and L representing the multipole order. $E_\gamma = E_i - E_f$ is the transition energy, $f_{XL}(E_\gamma)$ is the PSF for an XL transition, $\varrho_{XL}(E_i - E_\gamma)$ is the density of possible final states reachable from the initial state by a transition of type XL, and $\varrho(E_i)$ is the level density at the initial excitation energy. Regarding Eq. (5), it is obvious that the spectral shape of $Y_{{\rm bin},XL}(E_\gamma)$ is determined by two quantities: $\varrho_{XL}(E_i - E_\gamma)$ and $f_{XL}(E_\gamma)$. Figure 3 shows $Y_{{\rm bin},E1}(E_\gamma)$ calculated using the constant-temperature model (CTM) for the LD and a Lorentzian $E1$ PSF. The rise and fall of $Y_{{\rm bin},E1}(E_\gamma)$ is caused by the PSF rising with E_γ and the exponential decline of $\varrho_{XL}(E_i - E_\gamma)$.

In addition to primary γ rays, the complete neutron-capture γ-ray spectrum consists of higher order γ rays. If one knows the primary γ distribution, it is straightforward to calculate the distribution of secondary transitions. This distribution is the weighted superposition of primary γ distributions starting from different excitation energies populated after the first deexcitation step. In contrast, a derivation of an analytic expression for third- and higher-order γ rays is nontrivial. However, by using a Monte Carlo simulation for cascade deexcitations based on the primary γ-ray distribution [see Eq. (5)] the complete neutron capture spectrum can be simulated. For this purpose, we developed the statistical simulation code γDEX, which will be explained in detail in Sec. IV. The comparison of such simulated spectra with experimental data for the performed neutron capture experiment on ^{77}Se is discussed in Sec. IV B.

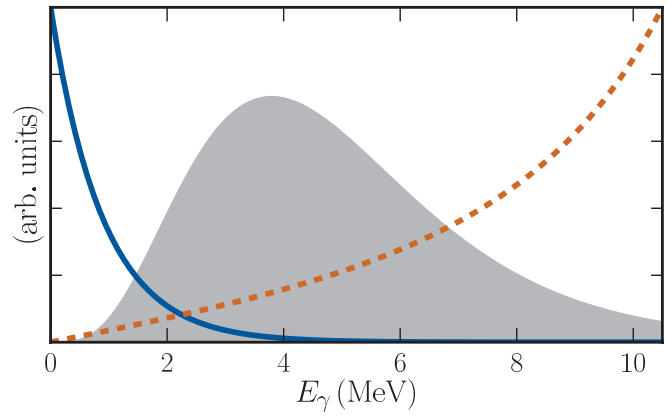

FIG. 3. (Color online) Spectrum of primary $E1$ transitions (gray area) from an excited state at 10.5 MeV as a product of the LD at the final state (blue solid line) and the E1 PSF (orange dashed line) given by the tail of the GDR. The LD is exponentially declining on this scale because it is plotted as a function of the transition energy E_γ. The scale of the ordinate is linear.

B. Photon-scattering γ spectra

As in the case of neutron capture, γ rays from excited states are measured in photon-scattering experiments. However, in contrast to neutron capture, various states of the target nucleus are excited in photon scattering using a continuous bremsstrahlung distribution for excitation. That means, if the endpoint energy of the bremsstrahlung distribution is above $S_{\rm n}$, the measured spectrum is a superposition of the deexcitation spectra of all excited states up to $S_{\rm n}$ if we assume that above $S_{\rm n}$, $\Gamma_{\gamma,{\rm n}} \gg \Gamma_{\gamma,\gamma}$, where $\Gamma_{\gamma,{\rm n}}$ is the partial width for photoneutron reactions and $\Gamma_{\gamma,\gamma}$ is the partial width for photon scattering.

Under the assumption of the extreme statistical ansatz of Sec. III A and the Axel-Brink hypothesis [13,14], the deexcitation spectra of the various excited states can also be calculated using Eq. (5). However, care has to be taken with regard to the influences of fluctuations in the transition widths. As will be shown in Appendix A, they lead to an enhancement of elastic (direct-ground-state) transitions. The simulation of deexcitation spectra in photon scattering is discussed in Sec. IV C. These simulations are used to determine the average photoabsorption cross section as presented in Sec. V.

IV. STATISTICAL SIMULATION OF RADIATIVE DEEXCITATION SPECTRA

A. General approach

For the description of radiative deexcitations of excited states at or below the neutron separation energy into the quasicontinuum region and to low-lying excited states, we developed the simulation code γDEX, which uses a fast and efficient computational approach shown in Fig. 4.

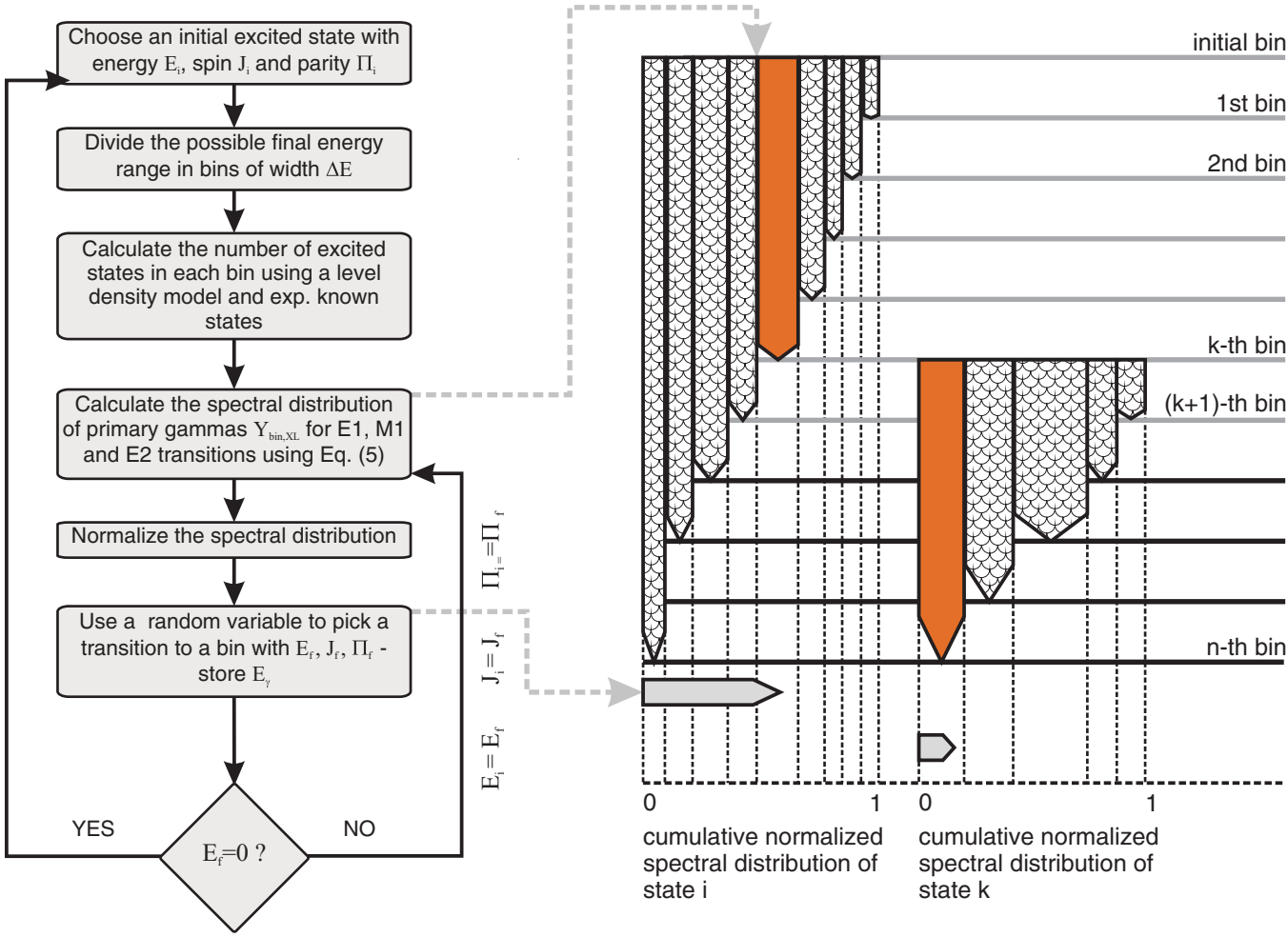

FIG. 4. (Color online) Block diagram and scheme of the algorithm for the simulation of nuclear radiative deexcitations.

First, the range of possible final energies is divided into bins of equal width (typically 200 keV). In each bin the number of possible final states is calculated for spins up to $J = 5$ (for an even-even compound nucleus) and both parities separately. Below 2.3 MeV these numbers are taken from the discrete level library in Ref. [6]. In our calculations, we used the energies, spins, and branching ratios of the first 10 excited states, which all have positive parity. Above 2.3 MeV, the total number of excited states is calculated according to a total LD. As standard input the CTM is used as a model for the total LD:

$$\varrho^{\mathrm{tot}}_{\mathrm{CTM}}(E) = \frac{1}{T} e^{(E-E_0)/T}, \tag{6}$$

where E is the excitation energy, E_0 is the back-shift energy, and T is the CTM temperature. Recently, it has been shown in Refs. [15–17] that this model describes the dynamics of different nuclear reactions such as energy transfer between fission fragments or particle evaporation spectra better than the back-shifted Fermi gas model (BFM). The three articles state that the CTM gives good agreement with experimental data up to excitation energies of S_n.

Above 2.3 MeV, we assumed equal LDs for states with positive and negative parities of the same spin. This assumption has recently been justified by the good agreement of calculated and experimental level densities of 1^+ states in the energy range from 5 to 10 MeV obtained from the ^{90}Zr(^{3}He, t)^{90}Nb reaction [18] and with experimental level densities of 2^+ and 2^- states in ^{90}Zr studied in ^{90}Zr(e, e') and ^{90}Zr(p, p') reactions [19]. In addition, the globally fitted empirical formula for the parity distribution given in Ref. [20] shows that the difference between the LDs for states with positive and negative parities of the same spin above 4 MeV is less than 3%. In the energy range between 2.3 and 4 MeV, the average relative difference between the parity distribution of Ref. [20] and our used equal distribution of positive and negative parities is 25%. It should be mentioned that recent calculations on the basis of Poisson-distributed independent quasiparticles combined with BCS occupation numbers predict different level densities for the two parities in ^{78}Sr below 7.5 MeV [21]. Nevertheless, we used an equal distribution of parities above 2.3 MeV in our calculations because Ref. [21] does not provide any parity ratios for ^{78}Se. For the spin distribution of states above 2.3 MeV the factor

$$f(J,\sigma) = e^{-J^2/2\sigma^2} - e^{-(J+1)^2/2\sigma^2} \tag{7}$$

derived in Ref. [22] is used, where σ is the energy-dependent spin cutoff factor taken from Ref. [23].

In the next step, the spectral distribution of primary γ rays is calculated according to Eq. (5) for $E1$, $M1$, and $E2$ transitions using models for the PSFs and information about possible final states in each bin from the above described LD model and experimentally known excited states. For the $E1$ PSF, the TLO [2], which describes the GDR as a sum of three Lorentzians corresponding to oscillations along the three axes in a triaxially deformed nucleus, is the standard input in γDEX. The $M1$ PSF was parametrized according to data from Ref. [24] as a sum of three Gaussian components corresponding to the scissors mode and the isoscalar and isovectorial spin-flip mode. The parameters of this $M1$ PSF are shown in Appendix B and a detailed discussion will be given in a further publication. The $E2$ PSF is calculated as a single Lorentzian according to Ref. [6].

After normalizing the total primary γ-ray distribution, a uniformly distributed random number is used to choose a final bin with a certain spin and parity for the γ transition. This procedure is repeated using the chosen final energy, spin, and parity as new starting properties until the ground state is reached. During the deexcitations, the transition energies and the energies, spins, and parities of the populated final states are stored.

The code γDEX developed in the present work has similarities but also different approaches compared with other codes such as DICEBOX [25], which was developed to simulate γ-ray deexcitations of excited nuclei with a statistical approach. The advantage of DICEBOX is the correct treatment of Porter-Thomas fluctuations [26] that may significantly influence the spectral shape, especially in regions with low level densities. The knowledge of the uncertainties in neutron capture γ spectra resulting from those fluctuations is necessary for a correct interpretation. On the other hand, due to the great number of excited states in medium and heavy nuclei up to S_n ($\approx 10^5$), many transition widths have to be calculated, making the computation very time consuming. Therefore, we developed γDEX, which uses a faster approach by calculating only transitions between energy bins containing several excited states.

We performed a test to check the consistency of both approaches by simulating the ^{77}Se(n,γ) spectrum with both codes using the same input PSF and LD. The simulation of neutron capture spectra with γDEX is explained in detail in Sec. IV B. The results of the consistency test are shown for comparison in Fig. 5, where it can be seen that the two computational approaches are in good agreement. Moreover, the comparison with DICEBOX allows us to estimate the uncertainties of the simulated spectra arising from fluctuations of the transition widths.

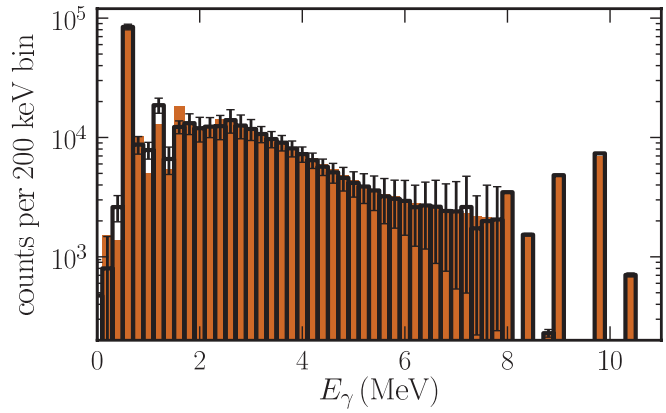

FIG. 5. (Color online) Simulated ^{77}Se(n,γ) spectrum using γDEX (orange bars) and DICEBOX (transparent bars with black edges and black error bars). In both cases identical CTM LD ($T = 900$ keV, $D_0 = 121$ eV) and PSFs were used. The DICEBOX spectrum is the mean of 200 nuclear realizations, each containing 10^5 simulated deexcitations. The error bars represent one standard deviation of the 200 realizations. The γDEX spectrum contains 10^6 simulated events and is normalized to the intensity of the transition at 10.5 MeV obtained in DICEBOX.

B. Simulation of neutron capture γ spectra

The code γDEX described in the previous section was used to simulate the measured ^{77}Se(n,γ) spectrum. However, the code was slightly adjusted to the conditions in cold neutron capture. As mentioned before, when using cold neutrons it is assured that only the capture state at S_n in the CN is excited. That means that the intensity in a typical 200-keV bin in the high-energy region of the measured spectrum results from single transitions of the initial excited resonance to the lowest-lying excited states. For these transition energies, the assumption made in Eq. (4) that the fluctuations of the transition widths cancel out clearly does not hold. Therefore the intensities of these transition energies are adjusted to experimental data taken from Ref. [9].

In contrast, the γ-intensity of a typical 200-keV bin in the continuum region can result from many different transitions, which assures that fluctuations in the transition width are averaged out. For example, for ^{77}Se(n,γ), a measured 4-MeV transition could be a primary transition from 10.5 to 6.5 MeV but also a secondary transition from 8 to 4 MeV or even a third-order transition.

To understand the influence of the main ingredients for the simulation, the LD and PSF, simulations of ^{77}Se(n,γ) with different models and parameters for LD and PSF were performed. In the first step, the influence of the level density was investigated by performing simulations with a CTM LD with different temperatures T in steps of 50 keV. The back-shift energy E_0 was calculated from the known mean s-wave neutron resonance spacing $D_0 = 121$ eV taken from Ref. [10] using Eq. (7) for the spin distribution at S_n. In these simulations we used a quadrupole deformation $\beta = 0.27$ [27] and a triaxiality parameter $\gamma = 27^\circ$ [28] for the TLO $E1$ PSF. The quadrupole deformation is compatible with the one deduced from experimental $B(E2)$ values in Ref. [29]. The simulated spectra are shown in comparison with the rebinned response-and-efficiency-corrected measured spectrum in Fig. 6 and are subdivided into primary, secondary, and higher-order transitions.

Regarding Fig. 6, a good agreement between the simulated spectra, which are normalized to the intensity of the direct-ground-state transition bin, and the measured spectra is visible. Furthermore, it can be seen that the γ-ray multiplicity of the

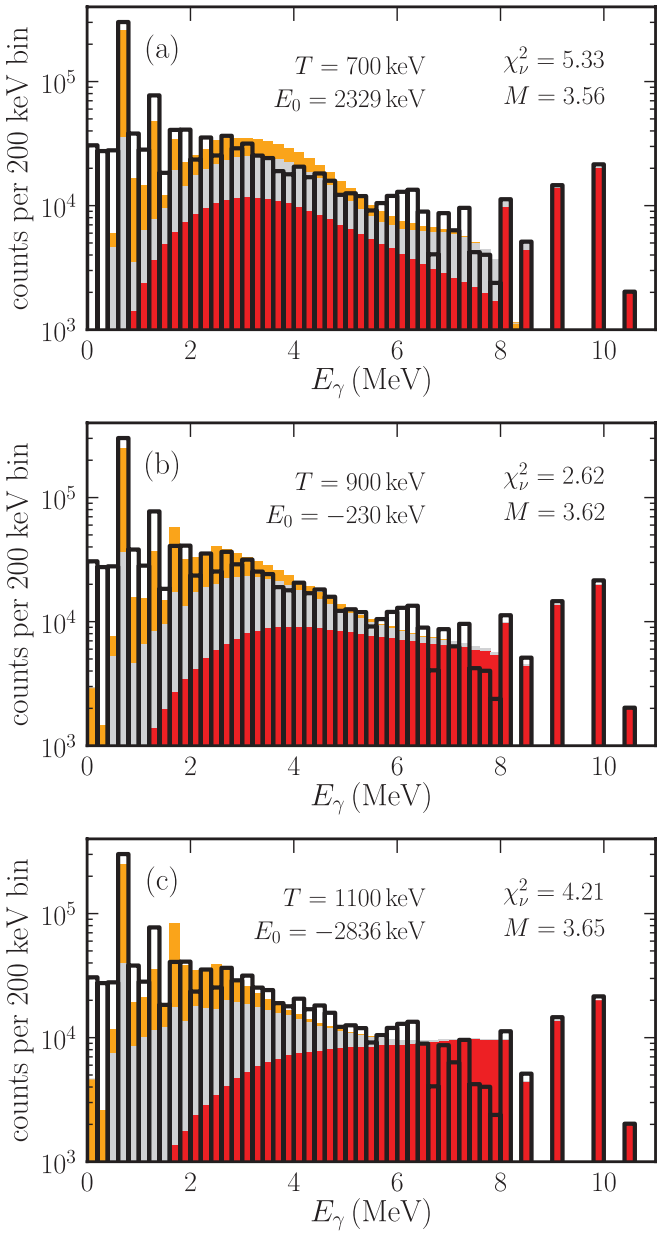

FIG. 6. (Color online) Rebinned experimental spectrum (transparent bars with black edges) corrected for detector response and efficiency in comparisons with simulated ^{77}Se(n,γ) spectra (colored bars) using different CTM temperatures. The simulated spectra are divided into primary (red bars), secondary (gray bars), and higher order γ rays (orange bars) plotted on top of each other. In all cases 10^6 deexcitations were simulated. The parameters (T and E_0) of the CTM LD model are 700 and 2329 keV in (a), 900 and -230 keV in (b), and 1100 and -2836 keV in (c). The back-shift energy E_0 was calculated separately for each T from $D_0 = 121$ eV using Eqs. (6) and (7) and a spin cutoff parameter $\sigma(S_n) = 4.4$.

reaction ^{77}Se(n,γ), $M \approx 3.6$, is only weakly dependent on T. With increasing T, the distribution of primary transitions gets broader and its mean is shifted to higher energies. Moreover, the slope of the continuum region ($2 \leqslant E_\gamma \leqslant 5.5$ MeV) of the total simulated spectra flattens. The goodness of fit between the simulated and measured spectra in this region is displayed

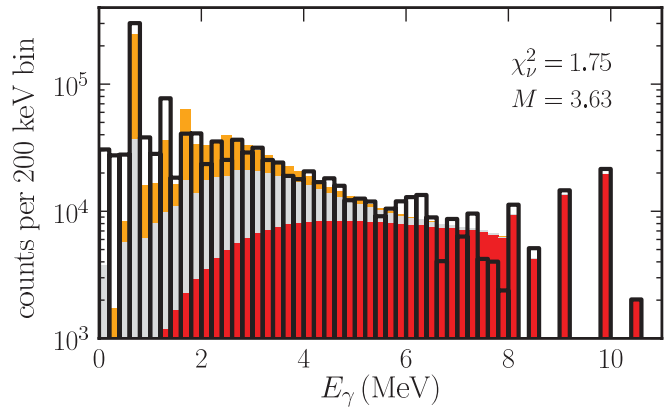

FIG. 7. (Color online) Same as Fig. 6 using a CTM LD with $T = 900$ keV and $E_0 = -230$ keV and the $E1$ PSF obtained in the (γ,γ') analysis shown in Fig. 11(b).

as χ^2_ν and was used to estimate T for the CTM LD. For the calculation of χ^2_ν we estimated a relative uncertainty of 10% for the simulated spectra in the energy region $2 \leqslant E_\gamma \leqslant 5.5$ MeV arising from Porter-Thomas fluctuations. We obtained a value of $T = 900$ keV as best fit for the CTM LD temperature, which is in agreement with the values of 850 keV given in Ref. [23] and 890 keV given in [30].

In addition, we simulated the neutron capture spectrum using a CTM LD with the best-fit temperature $T = 900$ keV and the $E1$ PSF obtained from the analysis of the photon-scattering experiment described in Sec. V and shown in Fig. 11(b). The result of this simulation displayed in Fig. 7 is in better agreement with the experimental data compared to the simulations using the TLO $E1$ PSF.

However, it can be seen that the experimental spectrum exceeds all simulated ones in the energy region around 6.3 MeV. As visible in Fig. 5, the uncertainties arising from Porter-Thomas in this energy region are large (>50%). Therefore, it remains unclear whether the experimental extra intensity in this region has its origin in an enhanced PSF or LD or is a result of fluctuations.

C. Simulations of photon-scattering deexcitation spectra

In addition to the simulation of neutron capture spectra, γDEX was also used to simulate average deexcitation spectra of states in ^{78}Se excited via photon scattering. As shown in Ref. [31], average radiative deexcitation spectra for various excitation energies have to be simulated to deduce the average photoabsorption cross section $\langle\sigma_{\gamma,\mathrm{abs}}\rangle$ or the related dipole PSF from a photon-scattering experiment with bremsstrahlung. On the one hand, these simulations can be used to subtract inelastic transitions from the measured spectrum; on the other hand, they can be used to estimate ground-state branching ratios of states excited in photon scattering. However, in the simulation of photon-scattering deexcitation spectra, the influence of fluctuations in the transition width must be treated with care.

Equation (5), the basis for the calculations in γDEX, is able to predict the average ground-state branching ratio of excited states in an energy interval around a particular excitation

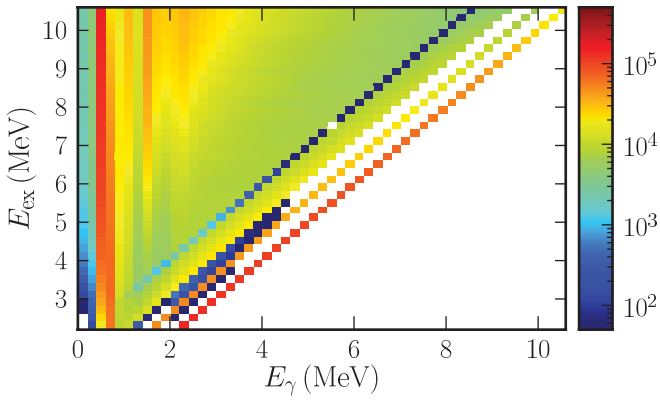

FIG. 8. (Color online) Simulated deexcitation spectra for excited 1^- states in ^{78}Se(γ,γ') in steps of 200 keV. For each excitation energy 250, 000 deexcitations were simulated. A CTM level density with $T = 900$ keV and an $E1$ PSF that was obtained from an iterative analysis of the photon-scattering data as shown in Fig. 11(b) were used as input parameters.

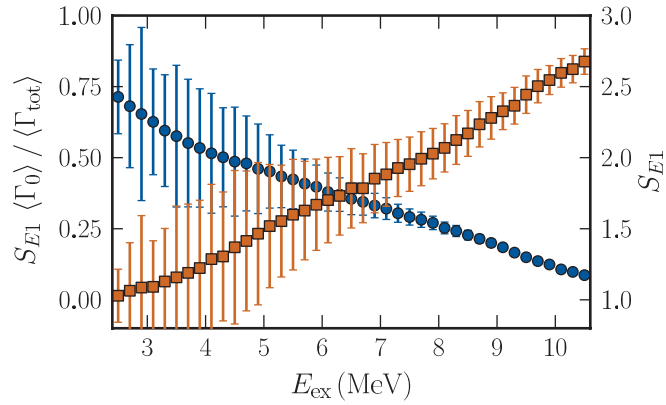

FIG. 9. (Color online) Simulated enhanced ground-state branching ratios (blue circles, left ordinate) and statistical fluctuation factors (orange squares, right ordinate) for excited 1^- states in ^{78}Se using the same LD and PSFs as in Fig. 8.

energy. This average ground-state branching ratio is an equally weighted average of the ground-state branching ratios of all states in the energy interval. However, in a photon-scattering experiment using bremsstrahlung, not all states in an interval around a certain excitation energy are excited with equal strength because of fluctuations in the transition widths. States with a large ground-state transition width will be excited with a higher probability than states with a small one. Subsequently, those states with a large ground-state transition width will decay with a higher probability directly back to the ground state than the other ones, leading to an enhancement of elastic photon scattering compared to other reaction channels. This phenomenon was already discussed in Ref. [32] for (γ, p) and in Ref. [33] for neutron-induced reactions.

The elastic enhancement effect in photon scattering can be described with an energy-dependent statistical fluctuation factor S mentioned in Ref. [12]. A method to calculate S is explained in detail in Appendix A. Simulated ^{78}Se(γ,γ') deexcitation spectra for excited 1^- states using γDEX and taking into account the effect of elastic enhancement are shown in Fig. 8.

This figure shows simulated deexcitation spectra using the best-fit CTM LD with $T = 900$ keV and $D_0 = 121$ eV taken from the analysis of ^{77}Se(n, γ) and an $E1$ PSF obtained from the iterative analysis of ^{78}Se(γ, γ) shown in Fig. 11(b). In the high-energy region of the simulated spectra, the ground-state transitions and the transitions to the lowest excited 0^+ and 2^+ states (diagonal structures) are visible. Moreover, in the low-energy region the transitions deexciting the lowest-lying excited states (vertical structures) can be seen. The enhanced ground-state branching ratios calculated in γDEX and the statistical fluctuation factors used are shown in Fig. 9.

The γDEX simulations predict mean ground-state branching ratios of approximately 8% at S_n (10.5 MeV), 35% at 6.1 MeV, and 62% at 3.1 MeV for excited 1^- states in photon scattering in ^{78}Se. The decrease of the branching ratio with increasing excitation energy is based on the exponential increase of excited states to which the initial state can deexcite. The displayed uncertainties in the enhanced branching ratio result from the uncertainties in the simulation of S explained in Appendix A. By using the simulated deexcitation spectra and ground-state branching ratios it is possible to calculate the average photoabsorption cross section from measured ^{78}Se(γ,γ') data, as will be discussed in the following section.

V. DETERMINATION OF THE AVERAGE PHOTOABSORPTION CROSS SECTION FROM THE PHOTON-SCATTERING EXPERIMENT

The energy-integrated photoabsorption cross section I_{abs} can be calculated for a target measured in photon-scattering experiments relative to the known integrated photoabsorption cross section $I_{abs,B}$ of a state in ^{11}B [34,35] at energy E_B by

$$\frac{I_{abs}(E, \Delta E)}{I_{abs,B}(E_B)} = \frac{Y_{abs}(E, \Delta E)}{N_T \, \Phi_E(E)} \times \frac{N_B \, \Phi_E(E_B)}{Y_{abs}(E_B)}, \qquad (8)$$

where Y_{abs} is the deduced number of photons absorbed in the target, N_T and N_B are the numbers of scattering target atoms and boron target atoms in the beam, and Φ_E is the spectral photon fluence at the target position. After a background subtraction, the measured photon-scattering spectrum contains elastic and inelastic transitions. From the measured number of counts, Y_{meas}, in a bin ΔE, the number of absorbed photons in the target can be determined by

$$\begin{aligned} Y_{abs}(E, \Delta E) &= \frac{Y_{elas}(E, \Delta E)}{B_0(E)\, S(E)\, W(\theta)} \\ &= \frac{Y_{meas}(E, \Delta E)/\varepsilon(E) - Y_{inelas}(E, \Delta E)}{B_0(E)\, S(E)\, W(\theta)}, \end{aligned} \qquad (9)$$

where Y_{elas} is the deduced number of elastically scattered photons from the target in a bin ΔE, Y_{inelas} is the simulated number of inelastically scattered photons from the target, $\varepsilon(E)$ is the total detector efficiency, $B_0(E)$ is the average ground-state branching ratio, $S(E)$ is the statistical enhancement factor discussed in Appendix A, and $W(\theta)$ is an angular correction coefficient that takes into account the angular distribution of the scattered photons. Thus, the following steps have to be

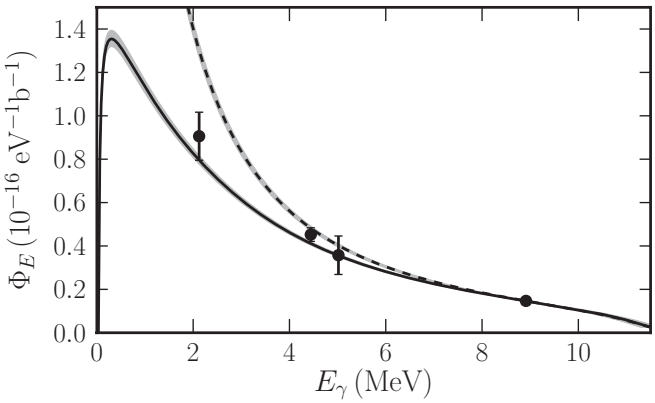

FIG. 10. Spectral bremsstrahlung fluence at the target deduced from four known transitions in ^{11}B (black circles) and the simulated detector efficiency. The dashed black line shows the calculated fluence distribution using the Seltzer and Berger formula [36]. The solid black line takes the influence of the aluminum hardener in front of the collimator into account. Both curves are normalized to the fluence at 8.92 MeV. The gray bands correspond to the uncertainty arising from a 200-keV uncertainty of the 11.5-MeV kinetic electron endpoint energy.

performed to determine the average photoabsorption cross section, which is related to the energy-integrated cross section from the measured photon-scattering data:

(i) Determine the photon fluence at the target position.
(ii) Subtract the room background.
(iii) Correct the measured spectrum for detector response and efficiency.
(iv) Subtract the non-nuclear (atomic) background.
(v) Subtract inelastic transitions and correct for branching, angular distribution effects, and elastic enhancement.
(vi) Normalize to a known cross section using Eq. (8).

The photon fluence at the target position shown in Fig. 10 was calculated according to the Seltzer and Berger formula [36] using a kinetic electron energy of 11.5 MeV. Moreover, the spectral shape was corrected for the influence of the Al hardener in front of the collimator. The absolute value was normalized to the fluence deduced from the 8.92-MeV ^{11}B transition. Figure 10 also shows the fluence values deduced from the other known transition in ^{11}B. The transition at 7.29 MeV has been omitted here since it shows a contamination by an unresolved transition in the measured spectrum. The total uncertainty in the photon fluence can be estimated to 9%, consisting of a 7.4% uncertainty in the fluence deduced from the ^{11}B transition and a 200-keV uncertainty in the endpoint energy.

In the next step of the analysis, a room background spectrum normalized by means of the 1.461-MeV transition in the decay of ^{40}K was subtracted from the measured spectrum. We simulated detector response spectra of incoming monoenergetic γ rays in steps of 10 keV using the program package GEANT4 [8] to correct the experimentally measured spectrum for detector response. The reliability of the simulated detector response is shown in Refs. [31,37]. The simulated detector response spectra were subtracted sequentially starting at the high-energy end of the measured spectrum, which was rebinned to 10 keV. Subsequently, the peaks resulting from the transitions in ^{11}B were subtracted.

Calibration source measurements with ^{60}Co and ^{226}Ra were performed to calculate the absolute detector efficiency. Additionally, GEANT4 simulations normalized to the calibration source measurements were used to determine the absolute efficiency in the energy range from 0 to 12 MeV. Measurements of (p,γ) reactions at the Tandetron accelerator at HZDR have shown that the simulated efficiencies are in agreement with the experimentally determined ones within their uncertainties of 5% up to energies of about 9 MeV [38].

Figure 2 shows the response-corrected experimental spectrum in comparison with the simulated atomic background which was calculated with GEANT4 and multiplied with the detector efficiency. In addition the spectrum resulting from a subtraction of the atomic background from the experimental spectrum is shown. As can be seen, the measured spectrum is dominated by the atomic background below 4 MeV, whereas at transition energies above 6 MeV the contribution of the atomic background is negligible. Moreover, a continuum of weak unresolved transitions that is clearly higher than the atomic background exists. This unresolved continuum is a consequence of the increasing LD and fluctuations in the transition widths, which lead to many weak unresolvable transitions.

As can be seen in Eq. (9), the contribution of inelastic transitions to the number of measured γ transitions has to be simulated and subtracted. For this purpose we used the code γDEX adjusted to the conditions in photon scattering to simulate average deexcitation spectra of 1^- and 1^+ states, excited by $E1$ and $M1$ excitations, respectively, from the ground state at different excitation energies as discussed in Sec. IV C. In the first step, the simulations were performed with a TLO $E1$ strength function, an $M1$ strength function consisting of three Gaussians, an $E2$ strength function described in Sec. IV A, and a CTM LD determined from the ^{77}Se(n,γ) analysis with $T = 900$ keV and $D_0 = 121$ eV, corresponding to $E_0 = -230$ keV using a spin cutoff factor of $\sigma(S_n) = 4.4$ [23]. Porter-Thomas fluctuations were used to simulate the statistical fluctuation factor S, describing the elastic enhancement in photon scattering. The simulated deexcitation spectra, the enhanced average ground-state branching ratio, and the statistical fluctuation factor are shown in Figs. 8 and 9.

After a step-by-step subtraction of the simulated inelastic transitions starting at the highest transition energy, the number of elastic transitions was obtained. Finally, we determined the number of absorbed photons by dividing the number of elastic transitions by the simulated enhanced average ground-state branching ratios and by the angular distribution correction factor $W(\theta)$. Subsequently, the average photoabsorption cross section was calculated using Eq. (8). Assuming that photoabsorption is dominated by dipole excitations, we obtained the dipole PSF f_1 using the relation derived in Ref. [12]:

$$\langle\sigma_{\gamma,\mathrm{abs}}\rangle = 3(\pi\hbar c)^2 E_\gamma f_1(E_\gamma). \tag{10}$$

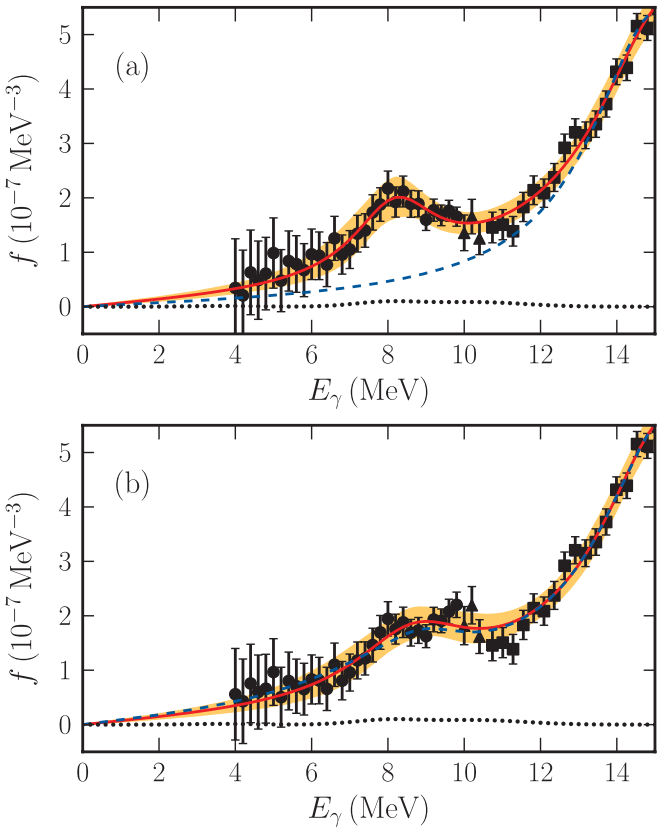

FIG. 11. (Color online) Iterative determination of the dipole PSF from photon scattering. The black circles are data from the (γ,γ') experiment corrected for inelastic transitions and branching. The black squares are (γ, n) data from Ref. [39] scaled with 0.85 following a proposal in Ref. [40]. The black triangles are the sum of (γ,γ') and (γ, n) in the region near the neutron threshold. The solid red line and the orange band are the deduced $E1$ PSF corresponding to a global fit and its 95% confidence interval to all data using a tail of the GDR plus an extra Lorentzian resonance. Since the correction for inelastic transitions and branching itself depends on the PSFs below the neutron threshold, the input $E1$ (blue dashed line) and $M1$ PSF (black dotted line) are shown for comparison. The values for the dipole PSF obtained in the first iteration using a TLO $E1$ PSF as input are shown in (a). Moreover, the results of the fourth iteration using an input $E1$ PSF fitted to the data of the third iteration are displayed in (b).

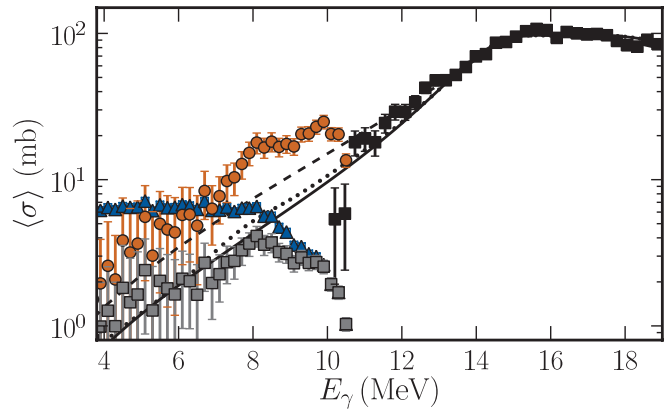

FIG. 12. (Color online) Cross section from uncorrected data (blue triangles), elastic photon-scattering cross section (gray squares), and photoabsorption cross section (orange circles) measured via photon scattering at HZDR in comparison with (γ, n) data from Ref. [39] (black squares) scaled with 0.85 following a proposal in Ref. [40]. In addition the prediction of the $E1$ TLO (black solid line) [2], $E1$ SLO (black dashed line) [6], and $E1$ TLO plus $M1$ (black dotted line) [24] models for the average photoabsorption cross section calculated from the PSFs are shown.

The deduced dipole PSF was compared to the ones used for the simulation of the deexcitation spectra which is shown in Fig. 11.

After the first iteration of the correction for inelastic transitions we found a discrepancy between the deduced PSF values and the ones used as input for the simulations of the number of inelastic transitions. Therefore, the obtained data from photon scattering were fitted together with the (γ,n) data from Ref. [39] scaled with 0.85 following a proposal in Ref. [40]. For the fit we used a PSF consisting of the tail of the GDR plus an extra Lorentzian. In the next step of the iterative analysis this fitted function was used as input for the simulation of the deexcitation spectra needed for the subtraction of inelastic transitions and the estimate of the ground-state branching ratios. This procedure was repeated until the input PSF for the simulations and output PSF from the (γ,γ') analysis were self-consistent.

We performed two different independent analyses. In the first one, the extra Lorentzian strength was assumed to be of $E1$ type whereas in the second one it was assumed to be of $M1$ type. As shown in Fig. 11, the resulting output data are only weakly influenced by the different input PSFs used in the single iteration steps, which is consistent with a test of various input PSFs in our earlier study of ^{90}Zr [41].

We obtained self-consistent results for the dipole PSF and the related average photoabsorption cross section after four iteration steps. The two different analyses just described yielded similar results. The mean deviation between the PSFs obtained in the two methods below S_n was found to be less than 15%. However, with respect to Ref. [24], an extra $M1$ strength of this magnitude seems unrealistic. The final elastic scattering and photoabsorption cross section deduced with the $E1$ analysis are shown in Fig. 12. The data not corrected for inelastic transitions and the measured (γ,n) cross section of ^{78}Se from Ref. [39] are shown for comparison. The (γ,n) data were scaled with a factor of 0.85 proposed in Ref. [40] and confirmed in Refs. [42,43]. In addition, the predictions of the TLO [2] and the standard Lorentzian model (SLO) [6] for the average photoabsorption cross section calculated from the $E1$ PSF are shown.

In the energy region just below S_n, the elastic scattering cross section coincides with the cross section obtained from the uncorrected data, because excited states there are not fed from above. States at lower excitation energies are strongly fed from cascade deexcitations of higher-lying excited states, which is why the elastic scattering cross section is lower than the uncorrected cross section in the low-energy region. The step-by-step subtraction of inelastic transitions from the flat

uncorrected data below 8.2 MeV leads to a local maximum in the elastic scattering cross section at 8.2 MeV (see Fig. 12).

The deduced average photoabsorption cross section exceeds that of the two pure Lorentzian models and shows broad enhanced strength around 9 MeV, corresponding to approximately 2% of the Thomas-Reiche-Kuhn sum rule. This extra strength is comparable to our earlier findings for ^{88}Sr, ^{90}Zr, ^{89}Y, and ^{139}La (see Refs. [31,41,44,45]).

VI. CONCLUSION

The level density and dipole strength function in the compound nucleus ^{78}Se have been studied in a combined analysis of a cold neutron capture experiment on ^{77}Se performed at the research reactor in Budapest and a photon-scattering experiment at the ELBE accelerator in Dresden using a kinetic electron energy of 11.5 MeV. For the analysis of both experiments we developed the extreme statistical code γDEX for the simulation of radiative deexcitation spectra of excited nuclear states. The analysis of ^{77}Se(n,γ) allowed us to estimate a CTM level density temperature of $T =$ 900 keV by comparing simulated and experimental spectra. In complementary fashion, this information about the level density in the compound nucleus ^{78}Se was used in connection with the code γDEX to determine the average photoabsorption cross section from the measured photon-scattering data.

In comparisons with different Lorentzian models for the GDR, extra strength was observed in a broad distribution around 9 MeV, corresponding to approximately 2% of the Thomas-Reiche-Kuhn sum rule as found in earlier (γ,γ') studies of ^{88}Sr, ^{90}Zr, ^{89}Y, and ^{139}La. This enhanced strength also fits the systematics of observed extra strengths in various nuclei investigated in Refs. [46] and [47]. Moreover, we achieved a very good agreement between the experimentally measured neutron capture spectrum and a simulated one using the PSF obtained from the analysis of the photon-scattering data.

It is very satisfying that a main aim of this investigation could be accomplished. By doing the neutron capture on a spin $1/2^-$ target nucleus, the differences in the spins of the states populated in neutron capture and in photon scattering were minimized. Under these conditions, it was possible to fit both the capture and scattering data with the same level density and the same $E1$ PSF, even including an anomalous contribution at 9 MeV. This is contrary to the belief that a different PSF is needed to fit the radiative capture from that which fits the photon scattering. It is our intent to further investigate the use of this technique of populating similar states with other nuclear pairs.

Furthermore, it could be shown that fluctuations in the transition widths lead to an enhancement of elastic transitions in photon scattering compared to the prediction of the average branching ratio. This enhancement could be quantified in a statistical simulation discussed in Appendix A.

ACKNOWLEDGMENTS

We thank the staffs of the ELBE accelerator in Dresden and the Budapest Research Reactor for their cooperation during the experiments and A. Hartmann for technical assistance. The two experiments were supported by the EURATOM FP6 Project EFNUDAT (036434), the Hungarian project OMFB 0018/2006 NAP VENEUS05, and the German BMBF project TRAKULA (02NUK13A).

APPENDIX A: ELASTIC ENHANCEMENT IN PHOTON SCATTERING

Gamma spectroscopy measurements in nuclear physics at high excitation energies face the problem that the average level spacing is smaller than the energy resolution of commonly used HPGe detectors. Hence, the observed quasicontinuum can only be used to derive average quantities such as the average photoabsorption cross section. As shown in Ref. [32] for (γ,p) reactions and in Ref. [33] for neutron-induced reactions, fluctuations in the transition widths lead to an enhancement of elastic transitions compared to predictions of a calculated average ground-state branching ratio. This general phenomenon also occurs in photon scattering.

If the photon-scattering average ground-state branching ratio of states i in an interval Δ around a certain excitation energy is to be calculated, the quantity

$$B_0 = \frac{\langle\Gamma_{i0}\rangle}{\langle\Gamma_{i,\mathrm{tot}}\rangle}, \tag{A1}$$

which is the ratio of the average ground-state transition width $\langle\Gamma_{i0}\rangle$ to the average total radiative width $\langle\Gamma_{i,\mathrm{tot}}\rangle$, is a wrong estimate. This is because of the fact that in Eq. (A1) the transition widths of all states in Δ are weighted equally. However, in photon scattering, not all excited states in Δ are excited equally. Those with a large ground-state transition width because of fluctuations are excited with a greater probability than those with a small one. After the excitation, those states with a large ground-state transition width will also deexcite directly back to the ground state with a greater probability than the other ones. Hence, Eq. (A1) underestimates the average ground-state branching ratio of states excited in photon scattering. In order to quantify this underestimate, the average cross sections for photoabsorption and photon scattering have to be compared.

According to Ref. [48] the average cross section for photoabsorption of transition type XL is given by

$$\langle\sigma_{\gamma,\mathrm{abs},XL}\rangle = 3\left(\frac{\pi\hbar c}{E}\right)^2\langle\Gamma_{i0XL}\rangle\varrho(E_i), \tag{A2}$$

where E_i is the excitation energy, $\varrho(E_i)$ is the density of states i that can be excited with respect to the transition rules in the bin Δ around E, and Γ_{ijXL} is the transition width between the states i and j for an XL transition. The average is taken over all states i in Δ around E. Furthermore, the average cross section for elastic photon scattering of transition type XL is given by

$$\langle\sigma_{\gamma,\gamma,XL}\rangle = 3\left(\frac{\pi\hbar c}{E}\right)^2\left\langle\Gamma_{i0XL}\frac{\Gamma_{i0XL}}{\Gamma_{i,\mathrm{tot}}}\right\rangle\varrho(E_i), \tag{A3}$$

which takes into account that only a fraction of the excited states i deexcites directly back to the ground state. As

suggested in Ref. [12], Eq. (A3) can be formally rewritten to

$$\langle \sigma_{\gamma,\gamma,XL} \rangle = \langle \sigma_{\gamma,\mathrm{abs},XL} \rangle \frac{\langle \Gamma_{i0XL} \rangle}{\langle \Gamma_{i,\mathrm{tot}} \rangle} S_{XL} \tag{A4}$$

by defining the statistical fluctuation factor

$$S_{XL} = \left\langle \Gamma_{i0XL} \frac{\Gamma_{i0XL}}{\Gamma_{i,\mathrm{tot}}} \right\rangle \Bigg/ \left(\frac{\langle \Gamma_{i0XL} \rangle \langle \Gamma_{i0XL} \rangle}{\langle \Gamma_{i,\mathrm{tot}} \rangle} \right). \tag{A5}$$

This definition of S_{XL} is reasonable to use in order to deduce the average photoabsorption cross section from the average elastic scattering cross section which can be measured in photon-scattering experiments. For this purpose, the fraction $\langle \Gamma_{i0XL} \rangle / \langle \Gamma_{i,\mathrm{tot}} \rangle$ can be calculated using the relation between the average transition width $\langle \Gamma_{ijXL} \rangle$ and the PSF f_{XL} for transitions of type XL:

$$\langle \Gamma_{ijXL} \rangle = \frac{f_{XL}(E_\gamma)\, E_\gamma^{2L+1}}{\varrho(E_i)} \tag{A6}$$

and the definition of the total radiative width:

$$\Gamma_{i,\mathrm{tot}} = \sum_{j,XL} \Gamma_{ijXL}, \tag{A7}$$

where $E_\gamma = E_i - E_j$ is the transition energy and f_{XL} is the PSF for an XL transition. In order to evaluate the statistical enhancement factor S_{XL}, the expression $\langle \Gamma_{i0XL} \Gamma_{i0XL} / \Gamma_{i,\mathrm{tot}} \rangle$ has to be calculated. Assuming that the fluctuations of the transition widths follow a certain distribution we are justified in writing

$$\Gamma_{ijXL} = y_{ij} \langle \Gamma_{ijXL} \rangle, \tag{A8}$$

where y_{ij} is a random number from the distribution of the fluctuations. By taking the average over all N states i in a sufficiently small interval Δ such that $\langle \Gamma_{i0XL} \rangle$ is constant for all states in the bin, we obtain

$$\left\langle \Gamma_{i0XL} \frac{\Gamma_{i0XL}}{\Gamma_{i,\mathrm{tot}}} \right\rangle = \frac{\langle \Gamma_{i0XL} \rangle^2}{N} \sum_{i=1}^{N} \frac{y_{0i}^2}{\Gamma_{i,\mathrm{tot}}}, \tag{A9}$$

At very high excitation energies, where on the one hand the level density is very high such that N is large and on the other hand the total radiative width is the sum of many partial widths such that according to the central limit theorem it does not fluctuate strongly, we obtain

$$\left\langle \Gamma_{i0XL} \frac{\Gamma_{i0XL}}{\Gamma_{i,\mathrm{tot}}} \right\rangle = \frac{\langle \Gamma_{i0XL} \rangle^2}{N \langle \Gamma_{i,\mathrm{tot}} \rangle} \sum_{i=1}^{N} y_{0i}^2 = \frac{\langle \Gamma_{i0XL} \rangle^2}{\langle \Gamma_{i,\mathrm{tot}} \rangle} \langle y_{0i}^2 \rangle, \tag{A10}$$

which is equivalent to

$$S_{XL}(N \to \infty) = \langle y_{0i}^2 \rangle. \tag{A11}$$

That means, for the limiting case of $N \to \infty$, S_{XL} is given by the mean of the squared fluctuation distribution. Assuming a reduced χ^2 distribution with ν degrees of freedom for this distribution, we obtain

$$S_{XL}(N \to \infty) = 1 + \frac{2}{\nu}, \tag{A12}$$

which is 3 for Porter-Thomas fluctuations [26]. For the analysis of the performed photon-scattering experiments, S_{XL} must be calculated for excitation energies from several MeV to S_n for $E1$ and $M1$ excitations. In this energy region the assumptions made in Eq. (A10) do not hold. Therefore, S_{XL} has to be simulated in a statistical way. For this purpose a simulation code was developed that works in the following way:

(i) The simulation code generates a nuclear random level scheme, with N_tot states up to an energy $E + \frac{\Delta}{2}$ according to the nuclear level density. By assuming that photon scattering is dominated by $E1$ and $M1$ excitations and target nuclei with ground-state spin-parity 0^+ are used, only 0^+, 0^-, 1^+, 1^-, 2^+, and 2^- levels are distributed because only those states can be populated in a two-step process consisting of an $E1$ or $M1$ excitation and an $E1$ or $M1$ deexcitation.

(ii) All average transition widths $\langle \Gamma_{ijXL} \rangle$ between all excited states are calculated using Eq. (A6).

(iii) Each average transition width is multiplied with a random variable y_{if} drawn from a reduced χ^2 distribution with ν degrees of freedom.

(iv) The two quantities $\langle \Gamma_{i0XL} \Gamma_{i0XL} / \Gamma_{i,\mathrm{tot}} \rangle$ and $\langle \Gamma_{i0XL} \rangle \langle \Gamma_{i0XL} \rangle / \langle \Gamma_{i,\mathrm{tot}} \rangle$ are calculated, where the averaging is done over all 1^- states for $E1$ excitations or over all 1^+ states for $M1$ excitations in the bin $[E - \frac{\Delta}{2}, E + \frac{\Delta}{2}]$. By division of these last two quantities, the statistical fluctuation factor S_{XL} is obtained for elastic ground-state transitions for one random level scheme.

(v) The simulation algorithm is executed several times, each time with a new random scheme of excited states and new fluctuations of the transition widths. In the end the mean value for S_{XL} deduced from all random level schemes is taken. At low excitation energies the algorithm is executed 10000 times and at high excitation energies it is executed 50 times.

S_{XL} factors as a function of excitation energy simulated for $E1$ and $M1$ excitations in ^{78}Se are shown in Fig. 13. For all simulations the averaging was done over all $1^-/1^+$ states in

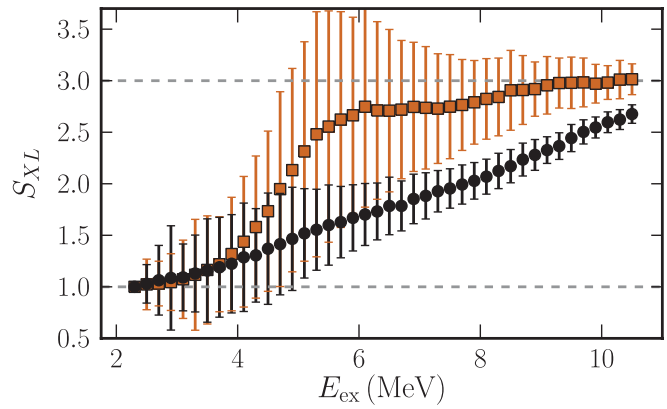

FIG. 13. (Color online) Statistical enhancement factor S_{XL} for $E1$ excitations (black circles) and for $M1$ excitations (orange squares) as a function of excitation energy simulated for ^{78}Se using the $E1$ PSF obtained from the analysis of the (γ,γ') experiment and $M1$ according to the data from Ref. [24] and a CTM LD with $T = 900$ keV and $D_0 = 121$ eV. The uncertainties correspond to one standard deviation of all runs performed for one excitation energy and the gray dashed lines indicate the asymptotic values for S.

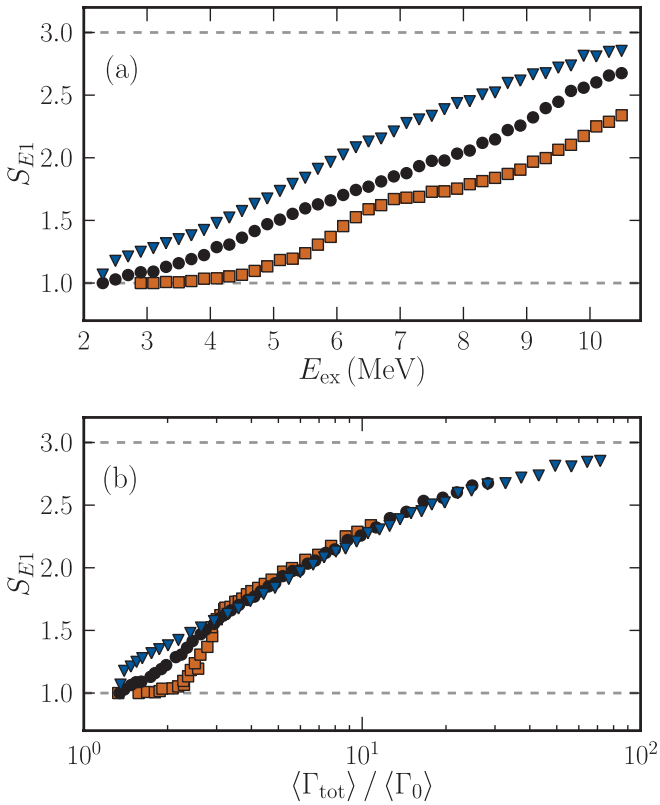

FIG. 14. (Color online) Statistical enhancement factor S for $E1$ excitations simulated with different CTM level densities with $T =$ 700 keV (orange squares), $T = 900$ keV (black circles), and $T =$ 1100 keV (blue triangles). For all simulations $D_0 = 121$ eV and the PSF shown in Fig. 11(b) were used. The uncertainties have been omitted for better visibility. (a) S as a function of the excitation energy. (b) S as a function of the ratio of the average total transition width to the average ground-state transition width. The gray dashed lines indicate the asymptotic values for S.

a 200-keV interval around the excitation energy. A CTM LD with $T = 900$ keV and $D_0 = 121$ eV was used to distribute the excited states in the random level scheme above 2.3 MeV. The spins of the excited states were assigned according to Eq. (7) with a spin cutoff factor taken from Ref. [23]. The distribution of states with positive and negative parity was assumed to be equal. Below 2.3 MeV we used the energies, spins, and parities of the first 10 excited states [6] in the level schemes. The fluctuation factors y_{ij} were drawn from a Porter-Thomas distribution. In the low-energy region ($E_{ex} \lesssim 3$ MeV), where on average there is approximately one state in the averaging interval, S_{XL} is close to unity. With increasing excitation energies, S_{XL} increases as well, until it reaches the limiting value of 3 at high excitation energies for the assumed Porter-Thomas distribution.

TABLE I. Parameters of the parametrization of the $M1$ PSF. Here, A_k is the amplitude, E_k is the peak energy, and σ_k is the standard deviation of the $M1$ component. Z is the atomic number, A is the mass number, β is the quadrupole deformation, and E_{GDR} is the centroid energy of the TLO $E1$ PSF given in Ref. [2].

Component	A_k (GeV^{-3})	E_k (MeV)	σ_k (MeV)
orbital/scissors	$(Z\beta)^2/62$	0.21 E_{GDR}	0.85
isoscalar spin-flip	$A/9.3$	34 $A^{-1/3}$	0.85
isovector spin-flip	$A/9.3$	44 $A^{-1/3}$	1.27

Figure 14 shows simulated fluctuation factors S_{E1} as a function of the ratio R of average total transition width to average elastic transition width, for different level densities. In regions where $R > 3$, approximately corresponding to $E_{ex} > 5.5$ MeV for ^{78}Se, S_{E1} as a function of R is independent of the LD. Furthermore, it can be seen that S_{E1} approaches 3 when R approaches infinity, which corresponds to very high excitation energies. However, in regions of very high R corresponding to excitation energies above the particle thresholds, other reaction channels are open. Thus the total width $\Gamma_{i,tot}$ contains also partial particle widths which influence S [32].

APPENDIX B: PARAMETRIZATION OF THE $M1$ PHOTON STRENGTH FUNCTION

The $M1$ PSF was parametrized according to the data of Ref. [24] as a sum of three Gaussians corresponding to the orbital and the isoscalar and isovector spin-flip mode:

$$f_{M1}(E_\gamma) = \sum_{k=1}^{3} A_k \, e^{\frac{-(E_\gamma - E_k)^2}{2\sigma_k^2}}. \qquad \text{(B1)}$$

Here, E_γ is the transition energy, A_k are the amplitudes, E_k are the peak energies, and σ_k are the standard deviations of the Gaussians. The parameter A_k, E_k, and σ_k are given in Table I for the three components.

[1] M. Salvatores and R. Jacqmin, NEA Technical Report 6410, 2008.
[2] A. R. Junghans, G. Rusev, R. Schwengner, A. Wagner, and E. Grosse, Phys. Lett. B **670**, 200 (2008).
[3] P. Ring and P. Schuck, *The Nuclear Many-Body Problem* (Springer, New York, 1980).
[4] J. Kopecky and M. Uhl, Phys. Rev. C **41**, 1941 (1990).
[5] T. Belgya *et al.*, *Handbook for the Calculation of Nuclear Reaction Data, RIPL-2*, (IAEA, Vienna, 2006).
[6] R. Capote *et al.*, Nucl. Data Sheets **110**, 3107 (2009).
[7] L. Szentmiklósi *et al.*, J. Radioanal. Nucl. Chem. **286**, 501 (2010).
[8] S. Agostinelli *et al.*, Nucl. Instrum. Methods A **506**, 250 (2003).
[9] Z. Révay *et al.*, *Handbook of Prompt Gamma Activation Analysis with Neutron Beams* (Kluwer Academic, 2004), Chap. Prompt Gamma-Ray Spectrum Catalog.
[10] S. Mughabghab, *Atlas of Neutron Resonances*, 5th ed. (Elsevier, Amsterdam, 2006).
[11] R. Schwengner *et al.*, Nucl. Instrum. Methods A **555**, 211 (2005).

[12] G. A. Bartholomew, E. D. Earle, A. J. Ferguson, J. W. Knowles, and M. A. Lone, Adv. Nucl. Phys. **7**, 229 (1972).
[13] P. Axel, Phys. Rev. **162**, 671 (1962).
[14] D. Brink, Ph.D. thesis, University of Oxford, 1955.
[15] M. Guttormsen, R. Chankova, M. Hjorth-Jensen, J. Rekstad, S. Siem, A. Schiller, and D. J. Dean, Phys. Rev. C **68**, 034311 (2003).
[16] A. Voinov *et al.*, Phys. Rev. C **79**, 031301 (2009).
[17] K.-H. Schmidt and B. Jurado, Phys. Rev. C **83**, 014607 (2011).
[18] Y. Kalmykov *et al.*, Phys. Rev. Lett. **96**, 012502 (2006).
[19] Y. Kalmykov, C. Ozen, K. Langanke, G. Martinez-Pinedo, P. von Neumann-Cosel, and A. Richter, Phys. Rev. Lett. **99**, 202502 (2007).
[20] S. I. Al-Quraishi, S. M. Grimes, T. N. Massey, and D. A. Resler, Phys. Rev. C **67**, 015803 (2003).
[21] D. Mocelj *et al.*, Phys. Rev. C **75**, 045805 (2007).
[22] T. Ericson, Adv. Phys. **9**, 425 (1960).
[23] A. Koning, S. Hilaire, and S. Goriely, Nucl. Phys. A **810**, 13 (2008).
[24] K. Heyde, P. von Neumann-Cosel, and A. Richter, Rev. Mod. Phys. **82**, 2365 (2010).
[25] F. Bečvář, Nucl. Instr. Methods A **417**, 434 (1998).
[26] C. Porter and R. Thomas, Phys. Rev. **104**, 483 (1956).
[27] S. Raman *et al.*, At. Data Nucl. Data Tables **78**, 1 (2001).
[28] W. Andrejtscheff and P. Petkov, Phys. Lett. B **329**, 1 (1994).
[29] R. Schwengner *et al.*, Z. Phys. A **326**, 287 (1987).
[30] T. von Egidy and D. Bucurescu, Phys. Rev. C **80**, 054310 (2009).
[31] R. Schwengner *et al.*, Phys. Rev. C **76**, 034321 (2007).
[32] P. Axel, K. Min, and D. Sutton, Phys. Rev. C **2**, 689 (1970).
[33] J. Lynn, *The Theory of Neutron Resonance Reactions* (Clarendon, Oxford, 1968).
[34] F. Ajzenberg-Selove, Nucl. Phys. A **506**, 1 (1990).
[35] G. Rusev, A. P. Tonchev, R. Schwengner, C. Sun, W. Tornow, and Y. K. Wu, Phys. Rev. C **79**, 047601 (2009).
[36] S. Seltzer and M. Berger, At. Data Nucl. Data Tables **35**, 345 (1986).
[37] G. Rusev *et al.*, Phys. Rev. C **77**, 064321 (2008).
[38] E. Trompler, Master's thesis, TU Dresden, 2009.
[39] P. Carlos *et al.*, Nucl. Phys. A **258**, 365 (1976).
[40] B. L. Berman, R. E. Pywell, S. S. Dietrich, M. N. Thompson, K. G. McNeill, and J. W. Jury, Phys. Rev. C **36**, 1286 (1987).
[41] R. Schwengner *et al.*, Phys. Rev. C **78**, 064314 (2008).
[42] C. Nair *et al.*, Phys. Rev. C **81**, 055806 (2010).
[43] M. Erhard *et al.*, Phys. Rev. C **81**, 034319 (2010).
[44] N. Benouaret *et al.*, Phys. Rev. C **79**, 014303 (2009).
[45] A. Makinaga *et al.*, Phys. Rev. C **82**, 024314 (2010).
[46] J. Endres *et al.*, Phys. Rev. Lett. **105**, 212503 (2010).
[47] T. Poelhekken *et al.*, Phys. Lett. B **278**, 423 (1992).
[48] P. Axel, in *Proceedings of the International Symposium on Nuclear Structure*, edited by Joint Institute for Nuclear Research, Dubna (International Atomic Energy Agency, Vienna, 1968), pp. 299–316.